





Cite this: *Soft Matter*, 2022, 18, 6222

Received 19th May 2022,
Accepted 15th July 2022

DOI: 10.1039/d2sm000661h

rsc.li/soft-matter-journal

Self-assembly and percolation in two dimensional binary magnetic colloids

Hauke Carstensen, Anne Krämer, Vassilios Kapaklis  and Max Wolff  *

We study the self-assembly of branching-chain networks and crystals in a binary colloidal system with tunable interactions. The particle positions are extracted from microscopy images and order parameters are extracted by image processing and statistical analysis. With these, we construct phase diagrams with respect to particle density, ratio and interaction. In order to draw a more complete picture, we complement the experiments with computer simulations. We establish a region in the phase diagram, where bead ratios and interactions are symmetric, promoting percolated structures.

1 Introduction

Self-assembly is the spontaneous formation of ordered structures on all length-scales¹ and a new route for the design of materials with complex functionality.² For small building blocks and finite temperatures entropy will allow a system to reach the global minimum in free energy and thermodynamic equilibrium. For systems dominated by the interaction between the constituents this may not be the case and the system can get trapped in a metastable state or become kinetically arrested.³

Colloidal systems consist of microscopic beads dissolved in a carrier liquid. Typically, the size of these beads is large and thermal energy becomes negligible. The systems' phase behaviour is defined by the interactions between the beads, making them interesting for the study of phase formation and self-assembly. By coating the bead surface with polymers, soft steric interactions may occur.⁴ More long-ranged interactions that are possible to realize are Coulomb interactions. The self-assembly of charged colloids was studied for beads of different sizes,⁵ aspect ratios⁶ and opposite charge.⁷ Even more rich in behaviour are magnetic interactions, since these are of dipolar nature and may be altered by external magnetic fields.⁸ The anisotropy of the interaction leads to the formation of clusters in the form of rings or chains with a head to tail orientation of the individual particles.⁹ With decreasing temperature or increasing density the size of such clusters increases and networks may form. These are challenging to study for nanometer sized particles as frozen samples are required for studies with transmission electron microscopy¹⁰ or computer simulations.^{11,12} For larger particles, the assembly process is easier to follow¹³ and rings,

chains and small networks were reported. Illustrative in this context is the study of cm-sized particles with different magnetic moments and their pattern formation and segregation.^{14,15} It was shown that by shaking and quenching magnetic particle systems larger open networks may be formed.^{16,17} All the above mentioned studies were performed without an externally applied magnetic field. Time dependent magnetic fields, however, allow precise tuning of the interactions¹⁸ and control of the self-assembly process¹⁹ as well as the study of the kinetics of self-assembly²⁰ and even the motion of self-assembled magnetic surface swimmers.²¹ By dispersing the magnetic beads in a ferrofluid matrix, an effective moment may be introduced, leading to tunable particle interactions. The local self-assembly of such systems was studied²² and a phase diagram of the local coordination was presented.²³ For two dimensional systems with an in plane magnetic field, depending on the interaction between the beads, cubic or hexagonal phases may form.²⁴

In certain applications, magnetic liquids are applied, for example, in loud speakers,²⁵ tunable photonic^{26–28} or plasmonic structures²⁹ and tunable shock absorbers.³⁰ These applications require knowledge on phase formation, not only on the local length-scales but also global, e.g. the formation of clusters or extended networks. On intermediate length-scales, colloidal crystals or networks may form, for which micrometer-sized particles allow tuning of the viscosity in the so-called magneto-rheological materials.^{31,32}

An important concept in this context is jamming, which allows relating changes in macroscopic material properties, e.g. viscosity, to topological constraints.³³ In the case of attractive interactions a phase diagram of jamming has been established³⁴ and it was shown that the jamming transition in systems with attractive and repulsive interactions fall into different universality classes.^{35,36} Similar to jamming, percolation may affect the macroscopic properties of a system. In the percolated state, all

Department of Physics and Astronomy, Uppsala University, Box 516, SE-75120, Uppsala, Sweden. E-mail: max.wolff@physics.uu.se



parts of a system are connected to each other. The jamming and percolation transition are characterised by critical densities.³⁷ The critical density for percolation was calculated for different coordinations in two and three dimensions³⁸ and is very similar to jamming happening at a critical random-close-packing density.³³ The influence of a long range repulsion and short range attraction on the percolation transition was investigated systematically using Monte-Carlo simulations.³⁹ These show that long-ranged repulsion increases the average cluster size and lowers the volume fraction for the percolation threshold.

In this communication, we report on the self-assembly and percolation of a binary, two dimensional system of magnetic beads with tunable interactions in an out-of-plane magnetic field. We classify the cluster formation with respect to the coordination of the individual beads, the crystal symmetry and percolation. We find that the critical density for percolation depends on the interaction between the beads and the bead ratio and report the lowest critical density for a bead ratio of 1:1 with attraction between the two species of beads and repulsion among beads of the same type.

2 Experimental details

Monodisperse micrometer-sized spherical particles (beads) – one magnetic and one non-magnetic – are suspended in a water-based ferrofluid. The beads, purchased from Microparticles GmbH, are made of polystyrene and have a diameter of 10 μm . The magnetic beads are covered by a shell of magnetic nano-particles. The ferrofluid (FF) consists of 10 nm iron oxide (Fe_3O_4) nanoparticles, dispersed in water and was purchased from LiquidResearch. In suspension, the beads exhibit an apparent magnetic behaviour mediated by the surrounding ferrofluid.^{24,40–42} The effective magnetic susceptibility of the suspended beads is modified by the susceptibility of the ferrofluid. This effect is in analogy to the concept of effective densities for objects in fluids, as described by the Archimedes principle, resulting in an apparent reduction of the susceptibility of the magnetic beads. The non-magnetic beads form magnetic voids in the ferrofluid matrix and may be assigned an effective magnetic susceptibility. By changing the concentration of magnetic nano-particles in the ferrofluid, the effective moments and thus the interaction between the beads can be tuned.

In the limit, $\chi_M \ll 1$ and $\chi_{\text{FF}} \ll 1$, with χ_M and χ_{FF} being the susceptibilities of the magnetic beads and the ferro-fluid, respectively, the effective bead susceptibilities $\chi_{M,\text{eff}}$ and $\chi_{N,\text{eff}}$ for the magnetic and non-magnetic beads, respectively, are:^{22–24,43}

$$\chi_{M,\text{eff}} \propto \chi_M - \chi_{\text{FF}} \quad (1)$$

$$\chi_{N,\text{eff}} \propto -\chi_{\text{FF}} \quad (2)$$

If the beads are confined along one dimension and a magnetic field is applied along the confinement direction, the interaction between the beads can be classified as follows:

- The interaction between identical beads is repulsive but tunable in strength, by changing the concentration of magnetic nano-particles in the ferrofluid.

- For $\chi_{M,\text{eff}} = 0$ and $\chi_{N,\text{eff}} = 0$ the magnetic and non-magnetic beads, respectively, are non-interacting.

The interaction between the two types of beads can be further modified in the following ways:²⁴

- For $\chi_{N,\text{eff}} < 0 < \chi_{M,\text{eff}}$ the coupling is anti-ferromagnetic and an attractive force is present between magnetic and non-magnetic beads.

- For $\chi_{M,\text{eff}} < 0$ and $\chi_{N,\text{eff}} < 0$ the interaction between all particles is repulsive.

This tunable interaction allows the systematical study of the structure formation in this binary system, with the ground states in the local ordering having been established previously.^{23,24,42,44} Here, we focus on the structure formation on larger length-scales and percolation phenomena.

The samples were prepared by mixing 20 μL of ferrofluid, 5 μL (1% w/w) of magnetic bead dispersion and 1 μL (2.5% w/w) of non-magnetic bead dispersion. This results in approximately equal numbers of magnetic and non-magnetic beads present in the sample. However, the beads may be inhomogeneously distributed and the local densities and ratios vary spatially within each sample. This enables the systematical study of the effect of density and bead ratio on self-assembly. To vary the interaction between the microbeads, a series of samples with varying FF concentrations were prepared. All of the samples were confined between two glass slides separated by an oil-covered 25 μm thick Mylar ring and studied by transmission optical microscopy. An out-of-plane magnetic field, with a maximum strength of 14 mT, was applied using a pair of Helmholtz coils. The magnetic flux density was calculated with finite element methods, implemented in FEMM.^{24,45} Fig. 1(a) shows a sketch of the experimental setup and the upper right panel results of the field calculation, indicating that the magnetic field is homogeneous over the area of the sample. The sample was loaded into the sample cell at zero field and all microscopy images were taken at an out-of-plane field of 0.14 mT. After loading the samples and before acquiring the images with the microscope, the field is cycled (switched on and off) repeatedly in order to reach an equilibrium structure. Subsequently, microscope images are recorded and bead positions are automatically extracted, identifying circular structures using image processing routines in MATLAB. The bead types are distinguished by their apparent brightness in the images. In addition, automatic detection was made more robust, utilizing a neural network algorithm trained on three images with labeled data (bead positions and types).

To complement the experiments, we performed computer simulations. Magnetic and non-magnetic beads are placed sequentially at random positions (without overlaps). The size of the simulated rectangular area was chosen to match the size of a typical microscopy image (50 \times 37 bead diameters) and periodic boundary conditions were applied. We further assume zero temperature, justified by the large size of the beads and the negligible Brownian motion as well as significant viscosity



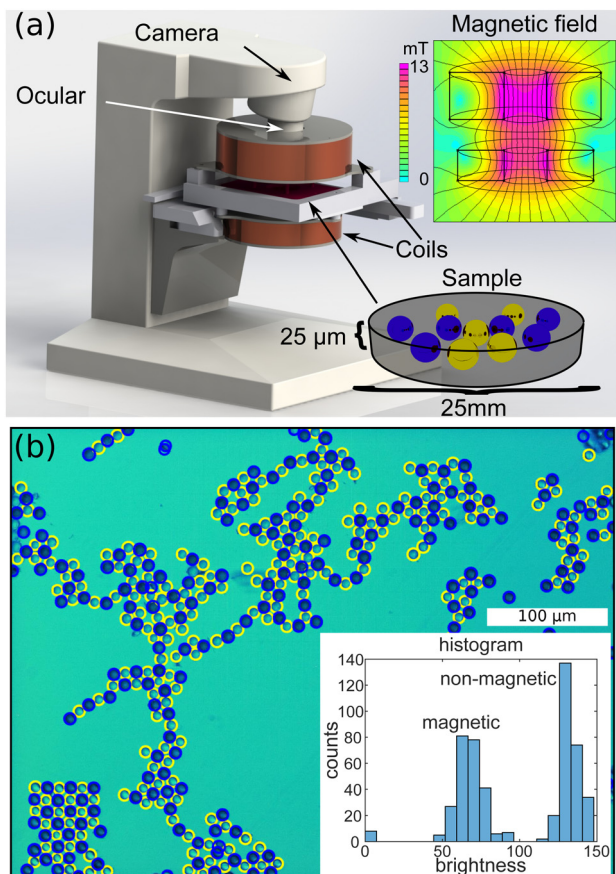


Fig. 1 Panel (a) depicts the transmission microscope setup. The panel to the upper right shows the magnetic flux density. Panel (b) is a typical microscope image with the magnetic and non-magnetic beads in darker and brighter colors, respectively. The particles have been identified automatically by evaluating their brightness (bottom right).

of the ferrofluid (zero bead momentum), no inertia and an overdamped equation of motion. The beads' magnetic moment is described as out-of-plane dipoles. To avoid overlapping of particles a hard sphere potential was used and particles are placed next to each other once they touch. In each simulation step the bead displacements are calculated from the force

acting upon each bead, resulting from the presence of all other beads, according to:

$$F_j = m_j c \sum_k \frac{m_k}{r_{j,k}^4} \quad (3)$$

where m_j and m_k are the dipole moments of beads separated by a distance $r_{j,k}$. As the dipolar forces decay rapidly with distance, we calculate the forces applying a cutoff of six bead diameters. Furthermore, the dipole force is scaled by $c = 0.01$ to keep the displacements in each step much smaller than one bead diameter. Our simulations minimise the total energy of the system and typically converge after 15000 iteration steps.

3 Results

Representative microscopy images are shown in Fig. 2 (top row). The bead density ρ defined as the image area coverage by beads, the bead type ratio $r = N_M/N_N$ where $N_{M,N}$ is the number of magnetic (M) and non-magnetic (N) beads, and the relative susceptibility χ_{FF}/χ_M , for which an image was recorded, is stated above each column of images. Panel (a) shows an image recorded for large values of χ_{FF}/χ_M . In this case the interaction between all beads is repulsive and they separate well. The blue beads (magnetic) are slightly closer to each other, as the force between them is smaller compared to the non-magnetic ones. No clustering or percolation is visible. Panel (b) was extracted for an equal bead ratio and $\chi_{FF}/\chi_M = 0.5$, resulting in the strongest attractive force between magnetic and non-magnetic beads. Two different beads have a strong tendency to stick together and tile. As the bead ratio is one, they form clusters with a four-fold symmetry. Panel (c) shows an image taken at a very unequal bead ratio and $\chi_{FF}/\chi_M = 0.33$. Beads of different kinds attract each other and organize in flower-like structures. However, the excess of one particle species cannot be fully compensated, leading to repulsion and many isolated beads. Panel (d) shows the case of an unequal bead ratio of 1/4 and $\chi_{FF}/\chi_M = 0.25$. As in panel (c), beads with a large effective moment are coordinated by the beads with a smaller moment. However, in this case the excess of one bead species is smaller

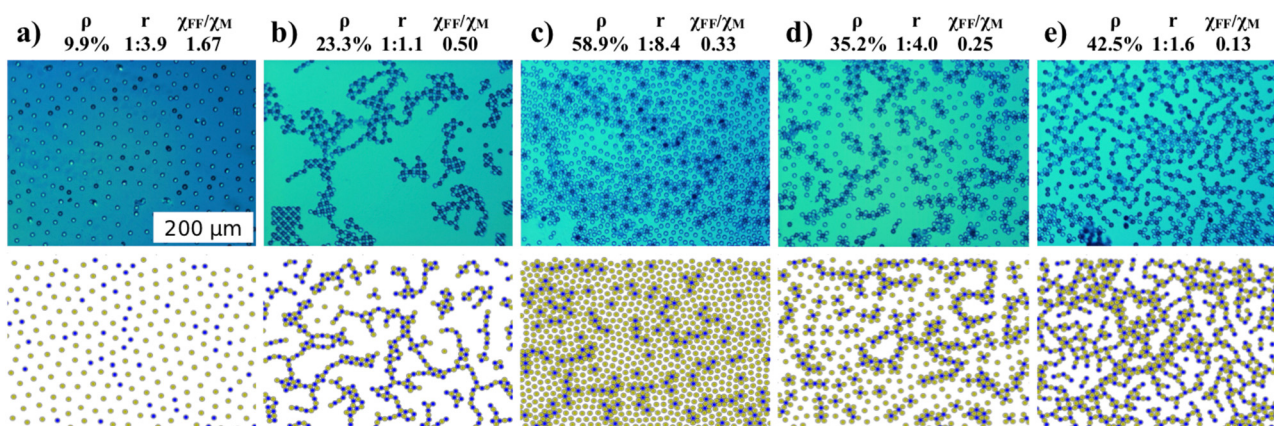


Fig. 2 Microscope images (top row) and simulated data (bottom row) for varying bead densities ρ , bead ratios r , and interactions χ_{FF}/χ_M .



and in a second step more beads with large dipole moments attach to the shell of the cluster. As a result larger clusters are formed with a local six-fold symmetry but still several isolated beads are visible. Panel (e) shows a picture taken with small $\chi_{\text{FF}}/\chi_{\text{M}}$ and a bead ratio close to one. Here it is possible to compensate for the differences in moment and the repulsion between clusters is overcome, forming networks or percolated structures. One might say that one type of bead is the glue keeping the other type, with repulsive interaction, together. The lower panels in Fig. 2 show computer simulations performed for identical parameters as in the upper panels. The simulations look similar to the microscope images, with slightly larger density fluctuations being present in the experimental data. Considering the good visual agreement we have performed more computer simulations and systematically varied all parameters, ρ , r and $\chi_{\text{FF}}/\chi_{\text{M}}$.

4 Discussion

Fig. 3(a) depicts the dipole energy per bead plotted as a color map over the bead ratio and relative susceptibility, for a bead density of 38.2%. This density was chosen as it is close to the critical concentration for percolation as explained later. Negative energies are regions in which the particles have a tendency to form clusters, while in the areas of positive dipole energies, they are isolated. The minimization of dipole energy results from competing attractive and repulsive interactions. Beads of identical magnetic susceptibility experience a repulsive force and the distance between them maximises to minimise the free energy. At the same time, magnetic and non-magnetic beads attract each other, compensating their collective moment and form an in-plane dipole giving rise to an anisotropic short-ranged force field in the plane (decaying faster than r^{-4}). The region of lowest energy is indicated by the white line and the white symbols denote the local minimum energy configuration of the beads, which arrange in square, honeycomb and kagome lattices for bead ratios r of 1:1, 1:2 and 1:3, respectively. The coordination number of the beads is shown in Fig. 3(c). In a chain each bead has two and for hexagonal packing six neighbors. For crystallisation or percolation an average coordination number of at least two is required and open networks may preferentially form for coordination numbers around three. A clear correlation is seen, between larger coordination numbers and low dipole energies per particle, being in line with the formation of large clusters for low dipole energies.

To analyse the coordination of individual beads in more detail, Fig. 3(d) shows the symmetry around beads. Blue, green and red colors indicate regions in which predominantly 6-fold, 5-fold and 4-fold symmetry is found, respectively. The intensity of the color represents how often the respective symmetry is found and quantified by the bond order parameter⁴⁶ for an s -fold symmetry, defined as $\phi_j = \frac{1}{n} \sum \exp(s \cdot i \cdot \theta_k)$, for each bead j having 3 or more neighbors, where θ_k are the angles of the connecting lines to direct neighbors, with respect to a reference vector. For beads with less than 3 neighbors, the

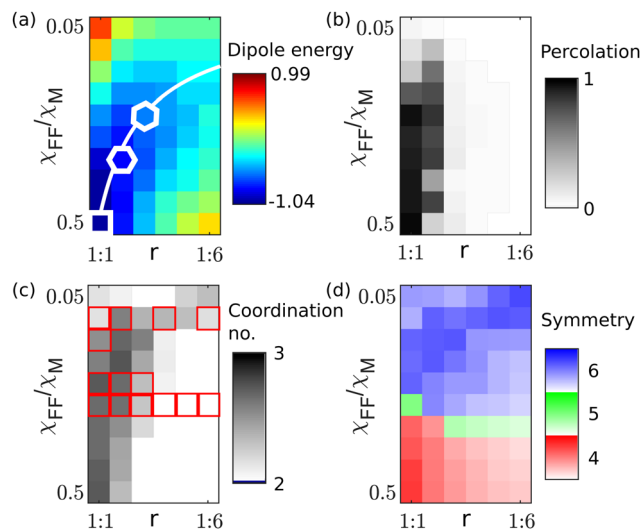


Fig. 3 Results from computer simulations performed for a bead concentration of 38.2%. Panel (a): dipole energy per bead plotted versus the bead ratio and relative susceptibility. The white line indicates the region of lowest energy and the symbols mark lowest energies for square ($r = 1:1$), honeycomb ($r = 1:2$) and kagome ($r = 1:3$) lattices. Panels (b), (c) and (d) represent the order parameter for percolation, the coordination of individual beads, quantified by the bond order parameter, and the most prominent symmetry, respectively. The red squares indicate parameters for which experimental data are available.

parameter is zero ($\phi_j = 0$). The average over all beads within one image is $\Phi_s = \langle |\phi_j| \rangle$ and is presented in the colormap. For the apparent moments of the beads being almost equal but of opposite direction four-fold symmetries are found. For highly asymmetric moments hexagonal packing is dominant. Interestingly the symmetry is almost independent of the bead ratio, as individual beads, which are left over, remain isolated. This relates well to the fact that large bond order parameters are found in regions of low average dipole moments. Another interesting observation is the five-fold symmetry found in the intermediate region. This symmetry hinders the formation of large crystals and should promote the formation of open networks and percolated structures. Fig. 3(b) depicts the percolation plotted as a map with respect to the bead ratio and relative susceptibility. To extract a percolation order parameter the average cluster size is weighted by the number of beads in each cluster, to become statistically more robust and is normalized to the total number of beads. This quantity can be used as an order parameter and varies between zero (isolated beads) and one (all beads connected). Clearly, highly asymmetric bead ratios do not form percolated structures, which are predominantly found for bead ratios of 1:1 and 1:2.

Fig. 3 presents results for a bead density of 38.2% but data have been evaluated for bead densities between 12.7% and 50.9%. Fig. 4 depicts the percolation order parameter plotted on a grey-scale versus bead density and interaction, for ratios of 1:1 (panel a) and 1:2 (panel b). The figure was created from simulations. Regions of predominantly hexagonal and cubic symmetry are identified for bond order parameters Φ_6 and Φ_4



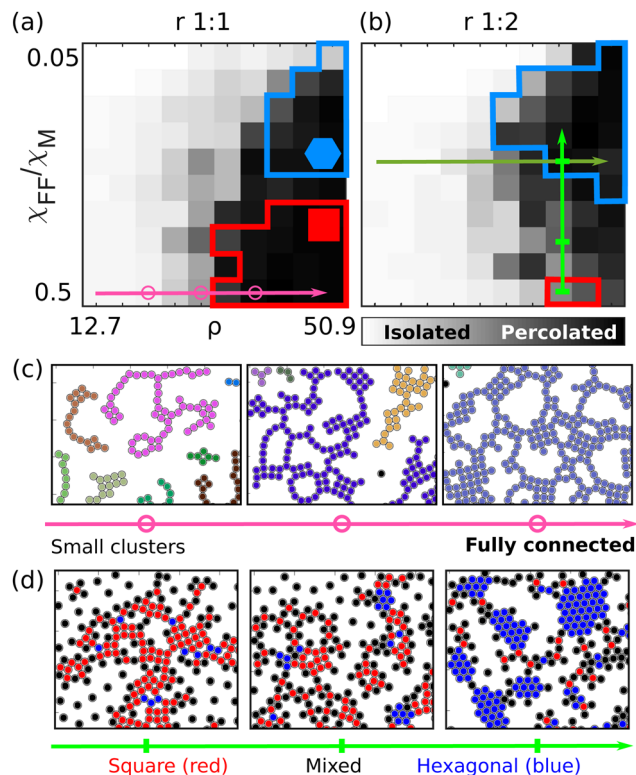


Fig. 4 The percolated, hexagonal and square phases plotted over interaction and density for ratios $r = 1:1$ (a) and $r = 1:2$ (b). (c) The transition from isolated beads to percolated with increasing bead density for $r = 1:1$. (d) The transition from square to hexagonal configuration with varying interactions for $r = 1:2$.

larger than 0.4, indicated by the blue and red colors, respectively. Fig. 4(c) depicts simulation images extracted for $\chi_{FF}/\chi_M = 0.5$ at three densities, indicated by the purple circles in Fig. 4(a). For low densities, clusters and/or chains form but do not connect to each other, as their mass is large and their total moment compensated. At higher densities crystallites form and become connected. Fig. 4(d) depicts the simulation images extracted for a density of 38.2% and three values of χ_{FF}/χ_M indicated by the green bars in Fig. 4(b). It turns out that in the intermediate region, where neither cubic nor hexagonal symmetry dominates, open percolated structures form, promoted by the large defect density (centre panel, Fig. 4(d)). The transition to percolated structures with respect to density is relatively sharp for all interaction parameters (Fig. 4(a and b)), allowing the extraction of the critical density for percolation, which is plotted *versus* χ_{FF}/χ_M in Fig. 5. Bead ratios of 1:1, 1:2 and 1:3 are marked by purple red and green colors, respectively.

The critical density for percolation has been calculated for triangles, squares, honeycomb and kagome lattices in two dimensions³⁸ and is in all cases close to 45%. For a bead ratio of 1:1 we find a lower value of the critical density for percolation, of about 30%, for $\chi_{FF}/\chi_M = 0.5$ (top right panel, Fig. 5). Here the interaction between the two species of beads is attractive and one type acts as glue for the other. The fact that the lowest critical density for percolation is found for values of

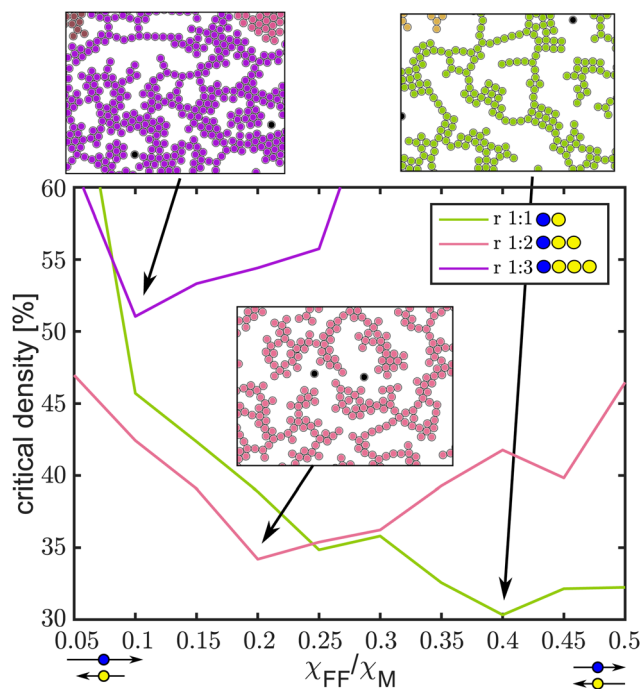


Fig. 5 Critical densities for percolation plotted *versus* interaction of magnetic and non-magnetic beads for bead ratios of 1:1, 1:2 and 1:3.

$\chi_{FF}/\chi_M < 0.5$ may be related to crystal tiling effects. At $\chi_{FF}/\chi_M = 0.5$ large cubic ($\rho \approx 79\%$) crystals form leading to larger critical densities for percolation, as it critically depends on the links between crystals. At small values of χ_{FF}/χ_M , the critical density for percolation becomes large ($>60\%$), as the repulsion between magnetic beads is dominating. A qualitatively similar behaviour is found for a bead ratio of 1:2, however, with the lowest value of the critical density for percolation found at lower χ_{FF}/χ_M . For a bead ratio of 1:3 percolation is only found for densities larger than 50%. The strong repulsion between the magnetic beads requires three non-magnetic beads to compensate, favouring hexagonal dense packed ($\rho > 90\%$) arrangements.

5 Conclusions

To conclude, we presented a statistical approach for analysing microscopy images and computer simulations, for extracting information on the self-assembly in a two dimensional binary colloidal dispersion with tunable interactions. Magnetic and non-magnetic beads are dissolved in a ferrofluid and investigated in an out-of-plane magnetic field. Depending on the concentration of magnetic nano-particles in the matrix the interaction between the two types of beads is repulsive or attractive. We find a low critical density for percolation, for attractive forces between the beads and bead ratios approximately equal to one, indicating the formation of extended and open networks. Our results are of high relevance for a range of research and technological fields, spanning across physics, chemistry, materials science, biology, epidemics and even



large-scale integration of nano-electronic devices.⁴⁷ Materials systems with controllable interactions, like the one presented here, can serve as an excellent model system as they allow for simple imaging of their microstates, providing statistically relevant information on the self-assembly and formation of percolating structures.

Author contributions

M. W, V. K and H. C together developed the conceptualization and methodology of the project. The investigations and formal analysis were performed by H. C and A. K. H. C also developed the software and validated and visualised the results. The project was supervised by M. W and V. K, who also acquired the funding and administered the project. The original draft was written by H. C and then edited by M. W and V. K and reviewed by all authors.

Conflicts of interest

There are no conflicts to declare.

Acknowledgements

We thank Niklas Johansson and Anders Olsson for constructing parts of the experimental setup. We acknowledge financial support from STINT (contract number: IG2011-2067), Swedish research council (contract number: A0505501), the Carl Tryggers Stiftelse (Contract number: CT 13:513) and the ABB group.

References

- G. M. Whitesides and B. Grzybowski, *Science*, 2002, **295**, 2418.
- G. M. Whitesides and M. Boncheva, *Proc. Natl. Acad. Sci. U. S. A.*, 2002, **99**, 4769.
- M. Klokkenburg, R. P. Dullens, W. K. Kegel, B. H. Erne and A. P. Philipse, *Phys. Rev. Lett.*, 2006, **96**, 037203.
- D. Qiu, T. Cosgrove and A. M. Howe, *Langmuir*, 2007, **23**, 475–481.
- R. Cademartiri, C. A. Stan, V. M. Tran, E. Wu, L. Friar, D. Vulis, L. W. Clark, S. Tricard and G. M. Whitesides, *Soft Matter*, 2012, **8**, 9771–9791.
- A. F. Demirörs, P. M. Johnson, C. M. van Kats, A. van Blaaderen and A. Imhof, *Langmuir*, 2010, **26**, 14466–14471.
- V. Kitaev and G. A. Ozin, *Adv. Mater.*, 2003, **15**, 75–78.
- D. Du, D. Li, M. Thakur and S. L. Biswal, *Soft Matter*, 2013, **9**, 6867–6875.
- S. Kantorovich, J. J. Cerda and C. Holm, *Phys. Chem. Chem. Phys.*, 2008, **10**, 1883.
- K. Butter, P. H. H. Bomans, P. M. Frederik, G. J. Vroege and A. P. Philipse, *Nat. Mater.*, 2003, **2**, 88.
- J. J. Weis and D. Levesque, *Phys. Rev. Lett.*, 1993, **71**, 2729–2732.
- S. Kantorovich, A. O. Ivanov, L. Rovigatti, J. M. Tavares and F. Sciortino, *Phys. Chem. Chem. Phys.*, 2015, **17**, 16601.
- W. Wen, F. Kun, K. F. Pál, D. W. Zheng and K. N. Tu, *Phys. Rev. E: Stat. Phys., Plasmas, Fluids, Relat. Interdiscip. Top.*, 1999, **59**, R4758–R4761.
- J. Stambaugh, D. P. Lathrop, E. Ott and W. Losert, *Phys. Rev. E: Stat., Nonlinear, Soft Matter Phys.*, 2003, **68**, 026207.
- J. Stambaugh, Z. Smith, E. Ott and W. Losert, *Phys. Rev. E: Stat., Nonlinear, Soft Matter Phys.*, 2004, **70**, 031304.
- D. L. Blair and A. Kudrolli, *Phys. Rev. E: Stat., Nonlinear, Soft Matter Phys.*, 2003, **67**, 021302.
- A. Krögel, P. A. Sanchez, R. Maretzki, T. Dumont, E. S. Pyanzina, S. S. Kantorovich and R. Richter, *Soft Matter*, 2018, **14**, 1001.
- A. T. Pham, Y. Zhuang, P. Detwiler, J. E. S. Socolar, P. Charbonneau and B. B. Yellen, *Phys. Rev. E*, 2017, **95**, 052607.
- R. Alert, J. Casademunt and P. Tierno, *Phys. Rev. Lett.*, 2014, **113**, 198301.
- A. V. Straube and P. Tierno, *Soft Matter*, 2014, **10**, 3915–3925.
- A. Snezhko, M. Belkin, I. Aranson and W. Kwok, *Phys. Rev. Lett.*, 2009, **102**, 118103.
- R. Erb, H. Son, B. Samanta, V. Rotello and B. Yellen, *Nature*, 2009, **457**, 999–1002.
- K. Khalil, A. Sagastegui, Y. Li, M. Tahir, J. Socolar, B. Wiley and B. Yellen, *Nat. Commun.*, 2012, **3**, 794.
- H. Carstensen, V. Kapaklis and M. Wolff, *Phys. Rev. E: Stat., Nonlinear, Soft Matter Phys.*, 2015, **92**, 012303.
- R. Rosensweig, Y. Hirota, S. Tsuda and K. Raj, *J. Phys.: Condens. Matter*, 2008, **20**, 204147.
- L. He, Y. Hu, H. Kim, J. Ge, S. Kwon and Y. Yin, *Nano Lett.*, 2010, **10**, 4708–4714.
- L. He, M. Wang, J. Ge and Y. Yin, *Acc. Chem. Res.*, 2012, **45**, 1431–1440.
- Y. Saado, M. Golosovsky, D. Davidov and A. Frenkel, *Phys. Rev. B: Condens. Matter Mater. Phys.*, 2002, **66**, 195108.
- F. Fan, S. Chen, W. Lin, Y.-P. Miao, S.-J. Chang, B. Liu, X.-H. Wang and L. Lin, *Appl. Phys. Lett.*, 2013, **103**, 161115.
- Q.-H. Nguyen and S.-B. Choi, *Smart Mater. Struct.*, 2009, **18**, 035012.
- B. J. Park, F. F. Fang and H. J. Choi, *Soft Matter*, 2010, **6**, 5246–5253.
- D. Wang and W. Liao, *Smart Mater. Struct.*, 2011, **20**, 023001.
- C. S. O'Hern, L. E. Silbert, A. J. Liu and S. R. Nagel, *Phys. Rev. E: Stat., Nonlinear, Soft Matter Phys.*, 2003, **68**, 011306.
- V. Trappe, V. Prasad, L. Cipelletti, P. N. Segre and D. A. Weitz, *Nature*, 2001, **411**, 772.
- J. A. Drocco, M. B. Hastings, C. J. O. Reichhardt and C. Reichhardt, *Phys. Rev. Lett.*, 2005, **95**, 088001.
- D. J. Koeze and B. P. Tighe, *Phys. Rev. Lett.*, 2018, **121**, 188002.
- D. Achlioptas, R. M. D'Souza and J. Spencer, *Science*, 2009, **323**, 1453.
- H. Scher and R. Zallen, *J. Chem. Phys.*, 1970, **53**, 3759.
- N. Valadez-Pérez, R. Castañeda-Priego and Y. Liu, *RSC Adv.*, 2013, **3**, 25110.
- A. T. Skjeltorp, *Phys. Rev. Lett.*, 1983, **51**, 2306–2309.



- 41 A. Skjeltorp, *Physica B+C*, 1984, **127**, 411–416.
- 42 H. Carstensen, V. Kapaklis and M. Wolff, *Eur. Phys. J. E: Soft Matter Biol. Phys.*, 2018, **41**, 9.
- 43 H. Carstensen, PhD thesis, Uppsala University, 2018.
- 44 Y. Yang, L. Gao, G. P. Lopez and B. B. Yellen, *ACS Nano*, 2013, **7**, 2705–2716.
- 45 D. Meeker, *Finite Element Method Magnetism (FEMM)*, 2021, <https://www.femm.info/wiki/HomePage>.
- 46 A. T. Pham, R. Seto, J. Schönke, D. Y. Joh, A. Chilkoti, E. Fried and B. B. Yellen, *Soft Matter*, 2016, **12**, 7735–7746.
- 47 G. Grimmett, *Percolation*, Springer-Verlag; New York, 1989.

